Noname manuscript No.
(will be inserted by the editor)

Prototype of a 4-Reaction Wheel System for Nanosatellites

Antoine Leeman

Received: date / Accepted: date

Abstract The overall procedure for building a reaction wheel is studied. A mechanical analysis is carried out to build a satellite simulator that includes four reaction wheels. A full characterization of a BLDC motor has been made, including the main mechanical and electrical parameters, the linear and non-linear models, the study of the saturation and finally the equations that drive the motor selection. An algorithm for a continuous speed and position estimation is proposed based on the measurements of the hall sensors. Then, the speed and torque control of a BLDC motor is studied and evaluated. Additional considerations for controlling a satellite such as the introduction of the Moore-Penrose Inverse Matrix are provided. This document also presents the different components needed to build the PCB to drive and control the BLDC motor in the core of the reaction wheel. We describe and explain the PCB to control a single motor and four motors. Finally, We validate all the previous results through extensive simulations.

Keywords Reaction Wheels · Control · Embedded system · Prototype · Electronics ADCS

1 Introduction

Reaction wheels are among the most common controllers of attitude for satellites. During the past years, an increasing number of nanosatellites, or CubeSats, have been sent into space.[1] Those nanosatellites can be used for education, technology demonstration, or nano-scale technology. As with any other kind of satellite, depending on the pointing accuracy and the requirements on

A. LEEMAN
ISAE-SUPAERO - 10 av. Edouard Belin - BP 54032 - 31055 TOULOUSE Cedex 4
Tel.: +33 5 61 33 80 80
Fax: +33 5 61 33 83 30
E-mail: antoineleeman@gmail.com

the maneuvers, the satellite may have an active or passive attitude control. The reaction wheels allow an active and accurate pointing accuracy independently of the environment or the orbit.[2][3] The Table 1 shows the main reaction wheels that can be found on the market today with a comparison of their specifications.

Table 1: Comparison of several reaction wheels on the market today [Source : Website of the companies]

	Sinclair Interplanetary	*CubeSpace The LaunchLab*		*Blue Canyon Technologies*		*Maryland Aerospace*
Name	RW-0.03	Medium	Large	RWP015	RWP050	MAI-400
Momentum $[N \cdot m \cdot s]$	40	10.82	30.61	15	50	11.076
Max Torque $[mN \cdot m]$	2	1	2.3	4	7	0.635
Mass $[g]$	185	150	225	130	240	110
Size $[mm]^3$	50, 50, 40	46, 46, 31.5	57, 57, 31.5	42, 42, 19	58, 58, 25	33, 33, 38

2 Mechanical design

2.1 Euler's equations

We can express the derivative of an arbitrary vector $\mathbf{A}$ in the inertial frame I knowing the rotating frame B and the rotation vector $\boldsymbol{\omega}$ using $\frac{d\mathbf{A}}{dt}\Big|^{I} = \frac{d\mathbf{A}}{dt}\Big|^{B} + \boldsymbol{\omega} \times \mathbf{A}^{B}$. It is important to define properly every frame when the problem involves rotation. In the present document, we consider only the rotation around the center of mass of the satellite and not the translation at that point. We have an inertial frame that stays fixed throughout the rotation of the satellite, as well as a rotating frame attached to the rigid satellite. In the equations used in this paper, the superscript refers to the frame of the vector. The subscript refers to either the satellite or the reaction wheels. Knowing that the angular momentum in the inertial frame varies when an external torque is applied to the body such that $\mathbf{T}^{s}_{\text{ext}} = \dot{\mathbf{h}}^{I}$, we can also know how the angular momentum in the satellite-fixed frame evolves. The general form of the equation is given by $\mathbf{T}^{s}_{\text{ext}} = \dot{\mathbf{h}}^{s} + \boldsymbol{\omega} \times \mathbf{h}^{s}$ and it can be applied to any problem. In our case, we can express the total angular momentum of the system including the satellite and the reaction wheels. In the equation:

$$\mathbf{h}^{s}_{s} = \mathbf{I}^{s}_{s}\boldsymbol{\omega}^{s}_{s} + \mathbf{h}^{s}_{w}, \tag{1}$$

we see that the total angular momentum of the satellite is made up of two parts; the rotation of the satellite's body and the angular momentum stored in the reaction wheels. Let us note that this equation does not depend on the number of the wheels. We can subsequently find that the external torques, the angular momenta of the flywheels and their derivatives influence the rotation speed of the satellite in an a priori non-trivial way. The following equation shows a coupling between the rotation speed of the reaction wheels and the rotation speed of the satellite.

$$\mathbf{T}^s_{\text{ext}} = \mathbf{I}^s_s \dot{\boldsymbol{\omega}}^s_s + \dot{\mathbf{h}}^s_w + \boldsymbol{\omega}^s_s \times \mathbf{I}^s_s \boldsymbol{\omega}^s_s + \boldsymbol{\omega}^s_s \times \mathbf{h}^s_w. \tag{2}$$

We can see from this equation that we will be able to apply a torque on the satellite by varying the angular momentum of the reaction wheels. The dynamics of the satellite's body can be seen as a system with inputs such as the external torques applied to the satellite, the angular momentum of the wheels and their variation. The outputs are the rotation speeds of the satellite. We understand at this point that by choosing properly the function $\mathbf{h}^s_w(t)$ we will be able to control the rotation speed $\boldsymbol{\omega}^s_s$ of the satellite and, in turns, its attitude.

2.2 Kinematics

There exist many ways to represent the attitude of a body with respect to a given frame. In aerospace engineering, mainly two ways are used to map the attitude of the body onto a set of numbers. The first option is the Euler angles. The attitude of the body is described by a combination of three rotations around body-fixed or inertial axes. The physical meaning of the 3 angles can be understood and read rapidly. However, for a specific set of rotations, the body encounters a singularity where the rotation is ill-defined and can be therefore numerically unstable. In this study, we will use quaternions instead. The quaternions are 4-dimensional numbers that generalise the complex numbers. A rotation of amplitude α around an axis $\mathbf{a}$ can be written simply with a quaternion as $\mathbf{Q} = [\cos(\alpha/2); a_1 \sin(\alpha/2); a_2 \sin(\alpha/2); a_3 \sin(\alpha/2)]^T$. As a rotating body has only 3 degrees of freedom, a single rotation can be expressed with an infinite number of quaternions. Therefore, we will limit ourselves to the sphere $|\mathbf{Q}| = \sqrt{q_0^2 + q_1^2 + q_2^2 + q_3^2} = 1$. Satisfyingly, a combination of rotations can be expressed as the multiplication of the corresponding quaternions. Quaternions make successive rotations easy to calculate. If we define $\mathbf{Q}$ as the current attitude of the satellite, $\mathbf{P}$ as the desired attitude and $\mathbf{E}$ as the relative rotation between the two former values, we find that $\mathbf{PE} = \mathbf{Q}$. If the desired attitude is the unit quaternion, we have $\mathbf{E} = \mathbf{Q}$.[4] Finally, we can understand that the same information is contained in its derivative as in the rotation vector $\boldsymbol{\omega}^s_s$. It is natural that there exists a relation between both. We have indeed:

$$\dot{\mathbf{Q}} = \frac{1}{2} \Omega(\boldsymbol{\omega}^s_s) \mathbf{Q} \tag{3}$$

where Ω is a 4×4 matrix that depends only on the rotation vector $\boldsymbol{\omega}^s_s$.

To complete the model of the satellite, we can introduce a simple model of accelerometer and magnetometer. Indeed, the sensors onboard the satellite

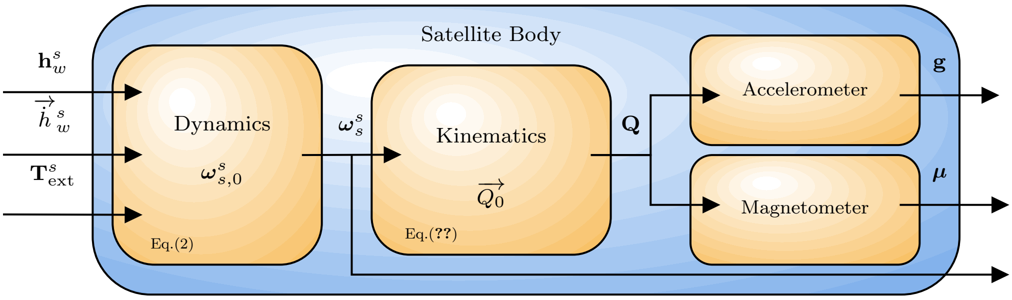

Fig. 1: Plan of the satellite used for the simulation. $\mathbf{Q}_0$ and $\boldsymbol{\omega}_{s,0}^s$ are the initial conditions.

won't indicate the attitude quaternion directly but measure the gravitational and magnetic field. We will explain later how to utilize the output of the accelerometer and magnetometer to control the satellite. Fig. 1 illustrates the full model of the satellite's body without the reaction wheels.

2.3 Motor

The key element of each reaction wheel is its motor. Understanding how the motor works and can be modelled, allowing better selection of the one that fits the need. An electric motor can be seen as an energy transformer. It converts electrical energy into heat and kinetic energy.

2.3.1 Mechanical saturation

The power used by the motor $P_{\mathrm{elec,mot}}$ is converted into electromechanical power P_{em} and Joule effect power $P_{\mathrm{J,mot}}$ with $P_{\mathrm{elec,mot}} = P_{\mathrm{em}} + P_{\mathrm{J,mot}}$. The power used by the motor can be approximated in steady state as $P_{\mathrm{elec,mot}} = U_{\mathrm{mot}} \cdot I_{\mathrm{mot}}$ where U_{mot} and I_{mot} are respectively the voltage applied to the motor and the current going through its winding. The electromechanical power of the motor can be expressed as $P_{\mathrm{em}} = T_{\mathrm{em}} \cdot \omega_w$ where ω_w is its rotation speed. T_{em} is actually divided into two parts. The first part of the torque will be used to counter balance the friction torque of the motor. We can find several ways to estimate the parameters of the friction model in the literature.[5][6] The second part of the torque will actually accelerate the flywheel. Finally, the Joule lost power is simply $P_{\mathrm{J,mot}} = R_{\mathrm{mot}} \cdot I_{\mathrm{mot}}^2$ where R_{mot} is the winding resistance. Considering that the current going trough the motor and the output torque are proportional in steady state $I_{\mathrm{mot}} \cdot k_M = T_{\mathrm{em}}$, we can obtain the following relation:

$$\frac{U_{\mathrm{mot}}}{k_M} = \omega_w + \frac{R_{\mathrm{mot}}}{k_M^2} \cdot T_{\mathrm{em}} \tag{4}$$

It means that for a given U_{mot}, we will have to choose between a high rotation speed or an high torque. As U_{mot} is bounded by the specification of the motor, this line defines a saturation on the T_{em} for a given rotation speed ω_w. As the rotation speed will constantly change, the value of the saturation will be dynamical. The higher the rotation speed, the lower the maximum possible torque will be.

2.3.2 Thermal saturation

The power lost in the motor due to the Joule effect will change the temperature of the motor. Assuming steady state, we see that the difference of temperature between the outside and the inside of the motor is given by $\Delta T = \sum_i R_{T,i} \cdot P_{\mathrm{J,mot}} = \sum_i R_{T,i} \cdot R_{\mathrm{mot}} \cdot I_{\mathrm{mot}}^2$ where $R_{T,i}$ is a thermal resistance. Assuming that we have a maximum difference of temperature $\Delta T_{\max}$, we can also calculate the corresponding torque with:

$$T_{t,sat} = \frac{1}{k_M} \sqrt{\frac{\Delta T_{\max}}{\sum_i R_{T,i} \cdot R_{\mathrm{mot}}}} \tag{5}$$

2.4 Requirements

To build a reaction wheel, it is also important to understand how the requirements of the mission of the satellite are linked with the specifications of the reaction wheel. Using a simple and unidirectional model for the satellite $(I_s - J)\ddot{\theta}_s = -T_w$(from [7]) where $T_w = T_{\mathrm{em}} - T_f$, we can write the torque necessary to perform a maneuver of θ_s during a time t^*. We have

$$T_w = 4\frac{I_s \cdot \theta_s}{t^{*2}}.$$

During that maneuver, the rotation speed and angular momentum will increase. We obtain therefore the angular momentum that the reaction wheel must have available:

$$h_{w,\max} \geq I_s \frac{\theta_s}{t^*} \tag{6}$$

At this point, we have to emphasize that those equations are approximations. We consider that the desired torque will be applied instantly, which is wrong. However, the equations can still give a preliminary knowledge on the final specifications of the reaction wheels.

2.5 Speed estimation

To control the speed of the reaction wheel, we firstly need to estimate it. If we use an encoder, the position of the motor is known relatively precisely at any time. It becomes easy to estimate its rotation speed. However, when the commutation of the electric motor is performed thanks to three Hall-effect sensors, the position is known only six times per revolution. But still, we need to know the position and the rotation speed of the motor at any time. We can then estimate those values at any time thanks to a Lagrange polynomial. We can estimate the position as a first order or second order polynomial and we obtain

$$\begin{aligned}\hat{\theta}_l(t) &= \theta_i \frac{t-t_i}{t_i-t_{i-1}} + \theta_{i-1}\frac{t-t_{i-1}}{t_{i-1}-t_i}\\ &= \frac{(\theta_i-\theta_{i-1})t-\theta_i t_i+\theta_{i-1}t_{i-1}}{\Delta T_1}\\ \hat{\omega}_l(t) &= \frac{(\theta_i-\theta_{i-1})}{\Delta T_1}\end{aligned} \tag{7}$$

$$\begin{aligned}\hat{\omega}_w(t) = \theta_i &\frac{(t-t_{i-1})+(t-t_{i-2})}{(t_i-t_{i-1})(t_i-t_{i-2})}\\ &+\theta_{i-1}\frac{(t-t_i)+(t-t_{i-2})}{(t_{i-1}-t_i)(t_{i-1}-t_{i-2})}\\ &+\theta_{i-2}\frac{(t-t_{i-1})+(t-t_i)}{(t_{i-2}-t_i)(t_{i-2}-t_{i-1})}\end{aligned} \tag{8}$$

$$\begin{aligned}\hat{\theta}_w(t) = \theta_i &\frac{(t-t_{i-1})(t-t_{i-2})}{(t_i-t_{i-1})(t_i-t_{i-2})}\\ &+\theta_{i-1}\frac{(t-t_i)(t-t_{i-2})}{(t_{i-1}-t_i)(t_{i-1}-t_{i-2})}\\ &+\theta_{i-2}\frac{(t-t_{i-1})(t-t_i)}{(t_{i-2}-t_i)(t_{i-2}-t_{i-1})}\end{aligned} \tag{9}$$

where $\hat{\theta}_l(t)$ and $\hat{\omega}_l(t)$ are the first order approximation and $\hat{\theta}_w(t)$ and $\hat{\omega}_w(t)$ are the second order. θ_i and t_i are the previous measured positions and associated times. We see that the first order approximation follows the intuition for the speed estimation.

2.6 Modelling

A complete analytical model of a BLDC motor is not trivial[8][9]. The model should comprise the electronic commutation of the motor and should therefore include a *Transformed Model Type d-q* which is out of the scope of this paper. Instead, we will use a numerical model for the simulations based on `MATLAB`®and `Simulink`®. The electromagnetic torque of the motor can be expressed as $T_{\text{em}} = \frac{e_a i_a + e_b i_b + e_c i_c}{\omega_w}$, where e_i and i_i are the voltage and current in each winding. We see from this equation that the torque and rotation speed are in competiton with each other to draw electrical power from the motor.

3 Control

3.1 Linearization

The are several ways to get a linearized model of the BLDC motor with commutation. First, we could use the equations from [8] and particularly the section called "Formal Linearization of BLDC Motor Drive" or we could use the complete description from [10]. However, a more straightforward way is to linearize the entire non-linear numerical model of the motor. We will command the motor with a step input of 24V, and we will take the rotation speed as the output. The simulation will be run for a sufficiently long time. Then, the System Identification Toolbox^{TM}of `MATLAB`®/`Simulink`®can provide the transfer function that links the input to the output. To provide a step function as an input is not an arbitrary choice. Indeed, the transfer function of a system is the Laplace transform of its step response. The step response contains all the frequency information of the system. The toolbox gives a 97.3% accuracy for the linearized model, and we can therefore use it reliably.

4 Control of the BLDC motor

The control of the BLDC motor is well studied and quite mature in the literature. We can find articles such as [11] that use MRAC (Model reference adaptive control) or Particle Swarm.[12] Other articles speak about fuzzy PID[13]. In [9], an anti-windup is studied. The most straightforward and easy to implement is to build a PID controller. We also want to be able to control the reaction wheel in rotation speed and torque. The input of the motor is the voltage applied. In reality, the voltage will be controlled thanks to the duty cycle of the PWM. The output of the motor can be its rotation speed. The input must never exceed the maximum voltage specified by the manufacturer.

4.1 Speed Control

The first step in designing the controller is to create a stabilizing inner loop on the speed; this is a classical approach. We are able to choose the gain Kd and the time constant τ of the diagram Fig.2.

Then, before adding an anti wind-up, we can choose the gain Ki and Kp thanks to a pole placement. We will choose a damping factor ξ big enough to avoid the overshoot and the saturation. However, the further we stray from $\xi = \sqrt{2}/2$, the larger will be the settling time.

The best way to act on the settling time is to change the pulsation ω_p of the pole placement. The higher the pulsation, the faster the response will be. The lower the pulsation, the more stable the system will be. However, when the pulsation is higher, the system will be more influenced by the noise because the gains are higher. Finally, we can choose the gain Kaw to enhance the stability region of this system with saturations. In Fig.3, we can see the Nichols/Bode plot as well as the time plot of the closed loop. We can see that the margins are comfortable since we have an infinite gain margin, a phase margin of $73.95°$ and a delay margin of $0.1189s$. We acknowledge that the time response is fast and precise. The system remains stable for a wide range of input even if it reaches the saturation.

We can see this estimated speed as a first-order holder combined with a band-limited noise. In Fig.4, we fixed the first-order holder to a sample time

T_{bl} to quantify its influence on the speed estimation. The sample time has to vary since the estimation is made faster when the motor rotates faster. We can see in Fig.4 that when T_{bl} is too big, the estimation of the speed $\hat{\omega}_w$ is not good and the speed of the motor ω_w is far from the command. When $T_{bl} = 0.035s$, the command varies rapidly but gives a precise rotation speed. This is the limit of the method. We recommend not to run at low rotation speed. We also see in Fig.5 that when the noise is significant, the estimation of the rotation becomes less precise and the command becomes more erratic.

4.1.1 Torque control

There exist many ways to control precisely the torque of a BLDC motor such as hysteresis current control, Direct Current Control (DTC)[14], Field Oriented Control (FOC)[15] and so on. The two latter are examples of vector control. To control precisely the torque, we must take advantage of a measure of the phase current and voltage. The current varies quickly, and we need one of the best MCUs (Microcontroller Unit) on the market to control the motor that way. Besides, a torque controller that implements DTC or FOC is less robust than our speed controller because it is more complicated. We chose a solution which was simple and robust, but not very accurate. The satellite will command the speed of the reaction wheel based on the command on torque thanks to:

$$\boldsymbol{\omega}_c^w = \int_0^t \hat{J} \cdot \mathbf{T}_c^w d\tau \tag{10}$$

We won't be as accurate as with a FOC or DTC controller as the controller introduced a bias. However, this solution is easier to implement, and the controller of the satellite can correct the lack of precision of this method. If we notice that the precision is too low, the next prototype will have to measure the current and to implement a vector controller. We link the precision of this method with the precision of the estimation of the inertia $\hat{J}$. We will estimate the torque that the reaction wheels apply on the satellite thanks to the following transfer function used in `Simulink`® ($\omega_c = 250rad/s$ and $\xi_c = \frac{\sqrt{2}}{2}$)

$$\frac{\hat{T}_w}{J\omega_w}(s) = \frac{s \cdot \omega_c^2}{s^2 + 2 \cdot \xi_c \cdot \omega_c \cdot s + \omega_c^2} \tag{11}$$

This estimation of torque is used only during the simulations and is not embedded.

4.2 Control of the full satellite

So far we have a model of the satellite with the reaction wheels. However, the torques that the reaction wheels apply to the satellite are not necessarily aligned with the principal axis of the satellite. Especially when we have more than three reaction wheels, we should use a configuration where they are not

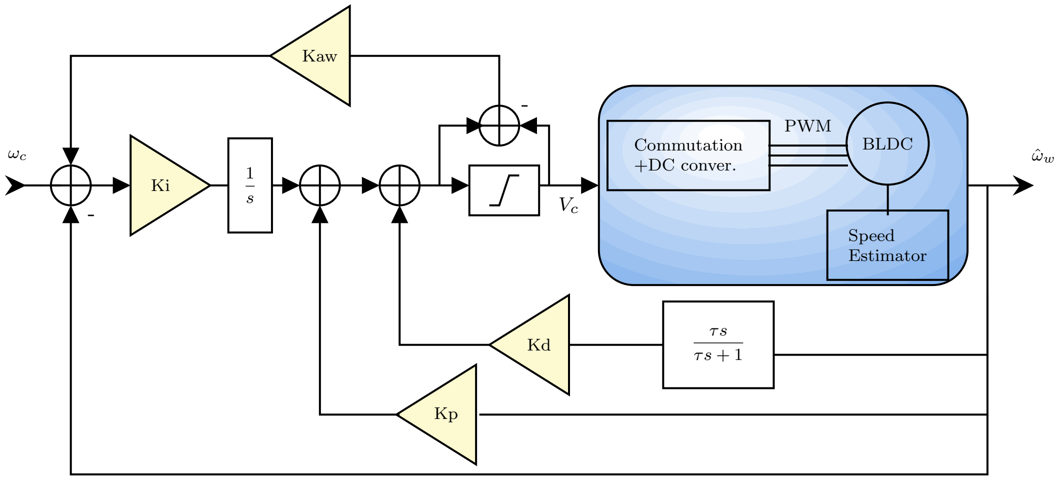

Fig. 2: Speed Control-loop of the BLDC motor

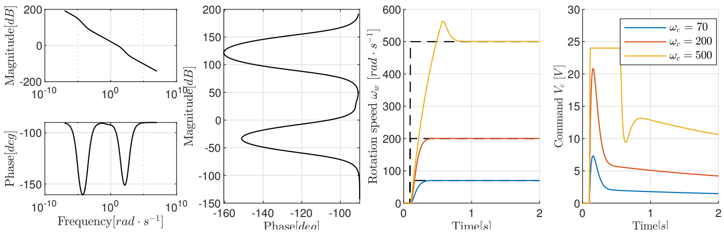

Fig. 3: Bode and Nichols plot of the PID controller (with $Kaw = 0$) shown in Fig.2. Time plot for different rotation speed commands (with $Kaw \neq 0$).

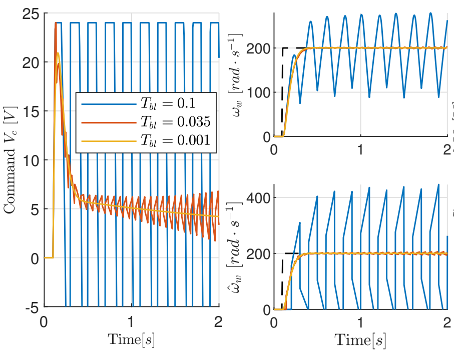

Fig. 4: Influence of the sample time of the speed estimation on the speed control. $\omega_{w,c} = 200$, $N_{power} = 0$.

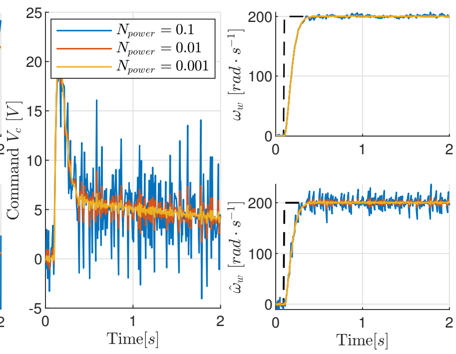

Fig. 5: Influence of the noise power N_{power} on the estimation of the rotation speed. $\omega_{w,c} = 200$, $T_{bl} = 0.01$.

aligned. If we want the satellite to survive the loss of a reaction wheel, it should still be able to rotate in any direction. In reference [16], we have a complete review of all the main configurations available. In particular, we have a list of matrices $\mathbf{A}_w$ that can link the torque generated by the wheels to the torque applied on the principal axis of the satellite:

$$\mathbf{T}_w^s = \mathbf{A}_w \mathbf{T}_w^w \tag{12}$$

where A_w is the reaction wheel configuration matrix defined as $\mathbf{A}_w = [a_{1,w}\ a_{2,w}\ a_{3,w}\ a_{4,w}]$ whereby $\mathbf{a_{i,w}}$ is the unit vector in the direction of the spin axis of the ith reaction wheel. On the other hand, if we want to apply the torque $\mathbf{T}_w^s$ to the satellite, we have to apply the torque $\mathbf{T}_w^w$ to the wheels $\mathbf{T}_w^w = \mathbf{A}_w^{-1}\mathbf{T}_w^s$. Likewise, we can write that $\mathbf{h}_w^w = \mathbf{A}_w^{-1}\mathbf{h}_w^s$ and $\mathbf{T}_c^s = \mathbf{A}_w\mathbf{T}_c^w$ where $\mathbf{A_w}^{-1}$ is the pseudo-inverse of the non-square matrix $\mathbf{A}_w$. To calculate the pseudo-inverse of a matrix is equivalent to minimizing the norm of the vector $\mathbf{T}_w^w$ which helps to avoid the saturation of the reaction wheels.

If we know the position of the accelerometer and magnetometer in the structure of the satellite, it is possible to infer the attitude quaternion based on the value displayed by the sensors. A singularity can appear at the poles, where the gravitational force aligns with the magnetic field. The algorithm introduced in the article [17] allows the inference of the attitude quaternion without any trigonometric calculation. This algorithm has been implemented in `Simulink`®and shows encouraging results. We can summarize this estimation function as $\mathbf{Q}_{\mathrm{mes}} = \mathcal{F}(\boldsymbol{\mu}, \boldsymbol{\gamma})$ with $\mathbf{g}$ and $\boldsymbol{\mu}$ respectively the gravitational and magnetic field measured by the satellite.

4.2.1 Control of the satellite

We can see the spacecraft as a MIMO system where the input is the control torque of the reaction wheels, and the outputs are the attitude quaternion and the rotation vector. Thanks to Lyapunov[18], we can show that the following attitude control stabilizes the satellite $\mathbf{T}_c^s = \mathbf{K}\mathbf{q}_e - \mathbf{C}\boldsymbol{\omega}_s^s$ where $\mathbf{q}_e$ is the vector part of the error quaternion, $\boldsymbol{\omega}_s^s$ is the rotation vector of the satellite and $\mathbf{T}_c^s$ is the torque command on the satellite. The matrices $\mathbf{K}$ and $\mathbf{C}$ can be either $\mathbf{K} = k_1\mathbf{I}_3\mathbf{C} = \mathrm{diag}(c_1, c_2, c_3)$ or $\mathbf{K} = \frac{k_2}{q_3^3}\mathbf{I}_3\mathbf{C} = \mathrm{diag}(c_1, c_2, c_3)$. In Fig. 6, we show a schematic representation of the full model used for the simulations.

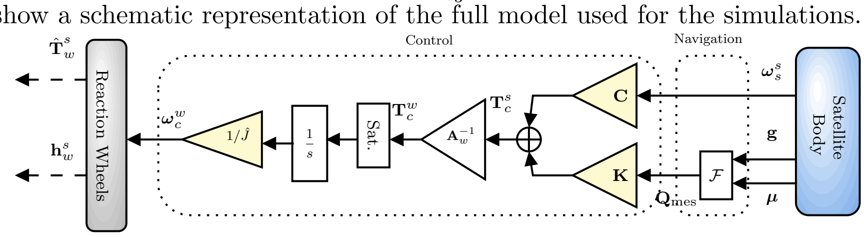

Fig. 6: ADCS used for the simulations. The dashed line represents a mechanical connection that is estimated using Eq.(11) for the simulations. The navigation could be improved with an Extended Kalman Filter.

5 Electronics and firmware

The electronics will have to perform several functions. In Fig. 7, we can see all the components that have been used. In a classical PCB, there two are kinds of lines. The first one carries power and the second one carries information. Generally, we try to transmit information with low power. We can see that the battery delivers a roughly constant voltage `VPWR`. However, the microcontroller needs a power supply of `Vcc`. The DC/DC converter will carry out the conversion. The Hall-effect sensors need a supply power of `Vhall`. The level charge pump will in turn provide this supply power. Then, the level shifter is used to convert the voltage of a quickly varying signal. It guarantees that no information is lost. A simple 9-DOF sensor is embedded on the PCB to allow improved testing and qualification of the whole system. The microcontroller will include the controller, provide the interface for communication with other parts of the satellite thanks to the UART, interpret the information of the Hall-effect sensors and send information about the commutation accordingly to the driver.

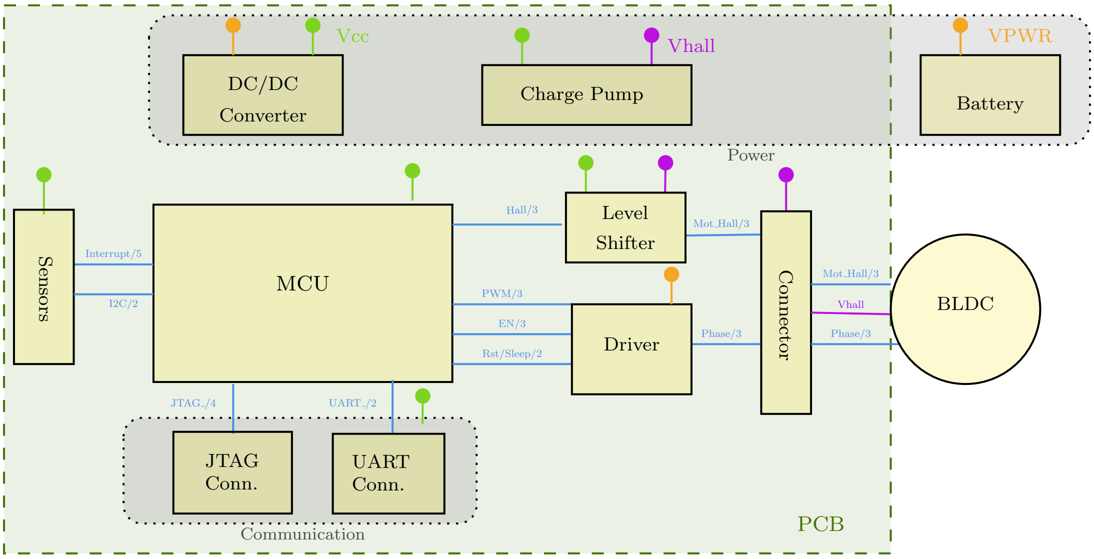

Fig. 7: PCB used to control a single motor

In Fig. 8, we propose a similar structure to control four BLDC motors. The architecture is the same as for a single BLDC but the authority of the full system is given to a FPGA. The FPGA is a logic gate circuit whose response time depends only on the propagation speed of the information. The code is not read and interpreted, it is propagated through the component. This element was chosen over a classical MCU because of the large quantity of information that has to be transmitted to each sub-PCB. It has to include the following services : commutation, controller, speed estimation and Pulse Width Modulation. Finally, we decided to divide the electronics among five different PCB to limit the consequences of a single fault.

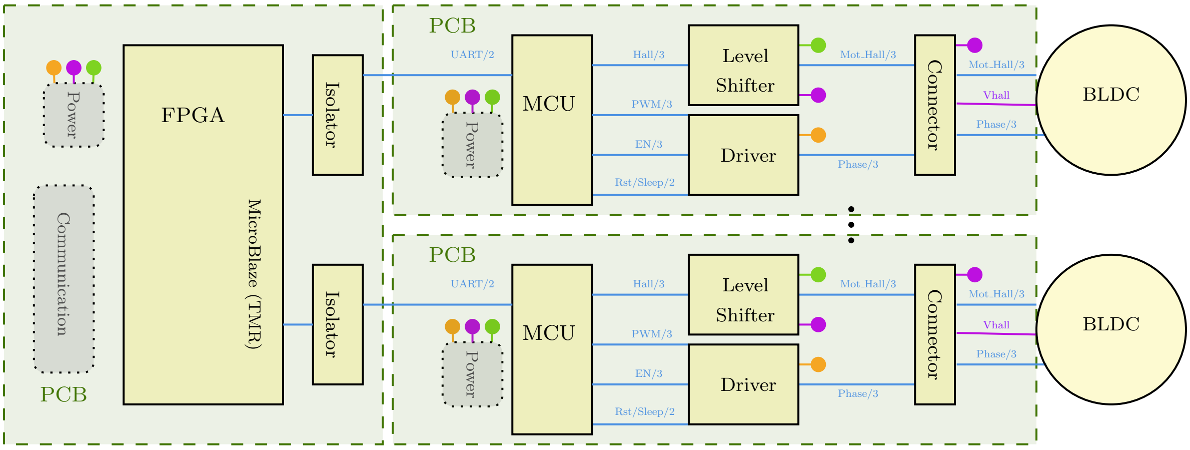

Fig. 8: PCB proposed to control 4 motors with improved reliability

6 Simulation

6.1 A single motor

We can simulate the behavior of the complete model of the reaction wheel and the control loop. We can compare the linearized system with the full non-linear models in Figs.9, 10 and 11. The efficiency is defined as $\eta = \frac{P_{\text{mech}}}{P_{\text{tot}}}$. We can see in those three figures that the linear model is a good approximation of the full model. The biggest difference arises with the commanded voltage. This difference is possibly due to the friction that is not modelled in the linear model. We can also see that there is a small difference in the efficiency that may be due to the same cause.

In Fig.9, we can see that the response time is quite fast for the torque. A step in torque is translated into a ramp in rotation speed. The command in rotation speed has a following error: we can see that the reaction wheel cannot hold a high torque for a long time since the saturation on the speed quickly moves closer. However, we reach a high enough angular momentum with $h_{w,\max} \approx 18mN \cdot m \cdot s$. We can also see that the precision on the torque is acceptable even with a very pessimistic estimation of $\hat{J}$. This assumption must be verified on the prototype in longer tests.

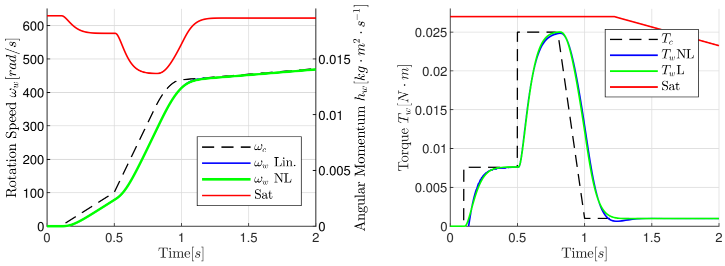

Fig. 9: Torque and rotation speed of the closed-loop reaction wheel.

In Fig.10, we can see the three different saturations: mechanical, thermal and on the voltage. We see that, even when the command is severe, the voltage is far from reaching the saturation.

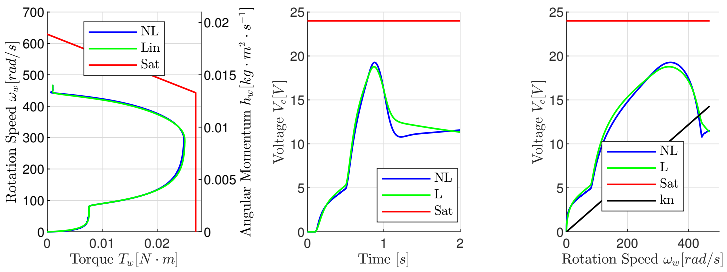

Fig. 10: Saturation of the reaction wheel.

We can see from the Fig.11 that the efficiency is poor at low speed and low torque. At the end of the maneuver, roughly 6J has been consumed, and a bit more than 3J was useful for the mechanics. The motor works best when the mechanical power needed is higher, which is a natural result. We can also see that we have a peak of total power of 12W which is indeed close to the saturation. The difficult command can explain this high power consumption. We can still use the reaction wheel at low torque to consume less energy. The temperature that the motor would reach in steady state conditions remains low at any time (lower than 50K of difference).

We can see in the Fig.12 that we obtain good performance. Our motor selection is correct because we can achieve the required maneuver in the given time for a classical nanosatellite. Besides, the control loop of the satellite is not optimized at all, meaning that we could achieve even better performance. The command starts with a high torque which rapidly gives a high rotation speed to the satellite. Then, the controller reduces the rotation speed thanks to a torque in the opposite direction. We can also point out the quality of the quaternion estimation method. The two lines are so close that we can

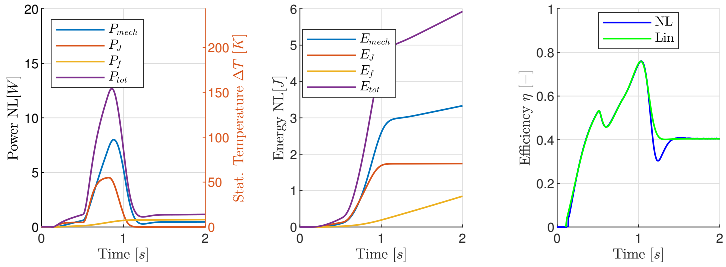

Fig. 11: Efficiency of the linear and non-linear model of the reaction wheel and power and energy consumed in the non-linear model.

barely notice the difference. The error on the estimation of the quaternion is a maximum of 0.005. We can also see that the satellite reaches its desired attitude smoothly. In Fig.13, we can see that the command is well below the saturation of 24V for this maneuver. The power required for this maneuver is quite high. The power required by the attitude control reached roughly 8W when the torque is the highest. If we want to reduce the required power, we must choose a slower maneuver. Concerning the efficiency of each reaction wheel, we can see that it becomes noisy for the second half of the simulation. Indeed, the estimation of torque created by the reaction wheel is not smooth. However, the satellite doesn't see those vibrations thanks to its high inertia and the quality of the simulation is not reduced. We see that the command voltage is not divided between the four reaction wheels. It depends on the position of each reaction wheel.

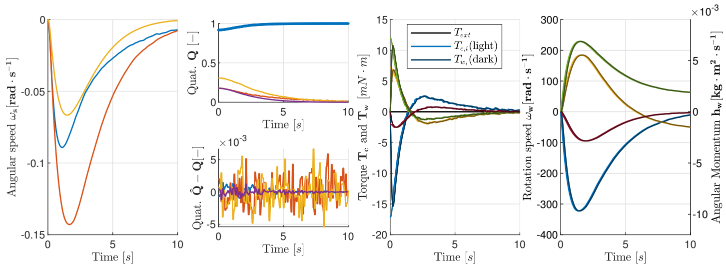

Fig. 12: The attitude quaternion, angular speed of the satellite, torque and rotation speed of the reaction wheels for the simulation of the full satellite.

7 Conclusion

Starting from the requirements on the maneuver of the satellite, we were able to build a 4-Reaction Wheel system. The project was divided into four main parts.

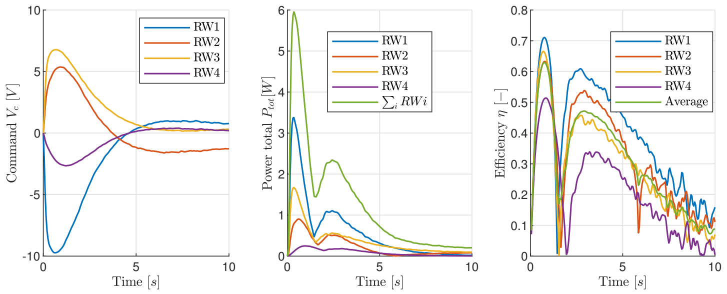

Fig. 13: The command, power, and efficiency of each of the four reaction wheels in the simulation of the full satellite.

Firstly, we built a mechanical model of the satellite and the motor which is difficult without a thorough a thorough understanding of the dynamics of the system as well as the electromechanical behavior of the BLDC motor. The model includes many details such as the non-linearities of the motor. This model allowed us to select an appropriate BLDC motor to meet the specifications. During the process of mechanical modeling, different `MATLAB`®toolboxes have been used such as System Identification Toolbox™, Aerospace Blockset™, Simscape™Power Systems™, and Simscape™Electronics™. The model of the motor is modular since it could be adapted to another BLDC motor with different specifications. All in all, the process of selecting a BLDC based on the requirements has become fast and accurate.

Secondly, we built the controller of the motor. The resulting controller is fast, precise and stable. We started by linearizing the model of the motor. Then, we added the PID and the anti-windup by carefully analyzing the temporal and frequential behavior of the closed-loop. We showed that the linear model was accurate, which allowed the acceleration of the design process of the PID.

Then came the design of the electronics component and the PCB. Building a PCB allows us to verify that all the simulations are correct even with the Processor-in-the-loop (PIL). Indeed, many projects may stop working because of a wrong estimation of delay times or calculation accuracy. Eventually, the plan of a reliable 4-motors PCB has been presented.

Finally, we ran the simulations of the reaction wheel alone. Thanks to those simulations, we could validate that the linear model was correct and that the controller kept the motor away from the saturation. The second part of the simulation uses the linear model of the motor to perform real maneuvers for the whole satellite that includes: the dynamical saturation of the BLDC motors, the noise of the accelerometer and magnetometer, the navigation algorithm that converts the data of the accelerometer and magnetometer into an attitude quaternion (from [17]), the speed and torque controller of the BLDC motor, the simple satellite controller, an estimation of the mechanical torque that the reaction wheels apply on the satellite and the detailed energy consumption of each reaction wheel.

Acknowledgements A special thank you to Hyochoong Bang and Mikal Marin from KAIST (Korea Advanced Institute of Science and Technology) for their continuous support and for letting me research on this topic in their lab.

References

[1]M. Swartwout, "The first one hundred cubesats: a statistical look", Journal of Small Satellites (2013).

[2]S. Jayaram, "Design and analysis of nano momentum wheel for picosatellite attitude control system", Aircraft Engineering and Aerospace Technology **81**, 424–431 (2009).

[3]M. J. Sidi, *Spacecraft dynamics and control: a practical engineering approach*, Cambridge Aerospace Series (Cambridge University Press, 1997).

[4]J. Diebel, *Representing attitude: euler angles, unit quaternions, and rotation vectors*, 2006.

[5]R. Kelly, J. Llamas, and R. Campa, "A measurement procedure for viscous and coulomb friction", IEEE Transactions on Instrumentation and Measurement **49**, 857–861 (2000).

[6]P. M. Kuo-Chia Liu and C. Blaurock, "Reaction wheel disturbance modeling, jitter analysis, and validation tests for solar dynamics observatory", in Aiaa guidance, navigation and control conference and exhibit (2008).

[7]J. J. H. Schaub, *Analytical mechanics of space systems*, 2nd ed., AIAA Education Series (AIAA, 2009).

[8]P. W. (auth.), *Dynamics and control of electrical drives*, 1st ed. (Springer-Verlag Berlin Heidelberg, 2011).

[9]M. Tariq, T. Bhattacharya, N. Varshney, and D. Rajapan, "Fast response antiwindup pi speed controller of brushless dc motor drive: modeling, simulation and implementation on dsp", Journal of Electrical Systems and Information Technology **3**, 1–13 (2016).

[10]N. Hemati and M. C. Leu, "A complete model characterization of brushless dc motors", IEEE Transactions on Industry Applications **28**, 172–180 (1992).

[11]A. A. El-samahy and M. A. Shamseldin, "Brushless dc motor tracking control using self-tuning fuzzy pid control and model reference adaptive control", Ain Shams Engineering Journal (2016) `https://doi.org/10.1016/j.asej.2016.02.004`.

[12]H. Ibrahim, F. Hassan, and A. O. Shomer, "Optimal pid control of a brushless dc motor using pso and bf techniques", Ain Shams Engineering Journal **5**, 391–398 (2014).

[13]A. Varshney, D. Gupta, and B. Dwivedi, "Speed response of brushless dc motor using fuzzy pid controller under varying load condition", Journal of Electrical Systems and Information Technology **4**, 310–321 (2017).

[14]M. Masmoudi, B. E. Badsi, and A. Masmoudi, "Direct torque control of brushless dc motor drives with improved reliability", IEEE Transactions on Industry Applications **50**, 3744–3753 (2014).

[15]T. I. Website, *1 may*, (2018) `http://www.ti.com/`.

[16]Z. Ismail and R. Varatharajoo, "A study of reaction wheel configurations for a 3-axis satellite attitude control", Advances in Space Research **45**, 750–759 (2010).

[17]X. Yun, E. R. Bachmann, and R. B. McGhee, "A simplified quaternion-based algorithm for orientation estimation from earth gravity and magnetic field measurements", IEEE Transactions on Instrumentation and Measurement **57**, 638–650 (2008).

[18]B. Wie, *Space vehicle dynamics and control*, 2nd Edition (American Institute of Aeronautics and Astronautics, 2008).